ELSEVIER

Full paper/Mémoire

One-pot synthesis to engineer a Co-KIT-6 catalyst for the ring opening of methylcyclopentane☆

Synthèse par voie directe d'un catalyseur Co-KIT-6 pour l'ouverture de cycle du méthylcyclopentane

Saida Debbih-Boustila [a, b], Ioana Fechete [a, *], Rabeh Kerbachi [b], Francois Garin [a]

[a] Institut de chimie et procédés pour l'énergie, l'environnement et la santé − ICPEES, UMR 7515 CNRS, Université de Strasbourg, 25, rue Becquerel, 67087 Strasbourg cedex 2, France
[b] École nationale polytechnique, Département "Génie de l'environnement", 10, avenue Hassen-Badi, B.P. 182, El Harrach, Algiers, Algeria

A B S T R A C T

Co-KIT-6 mesoporous materials with $Ia3d$ symmetry and Si/Co ratios of 50, 25, and 10 were prepared using hydrothermal one-pot synthesis. The Co-KIT-6 mesoporous materials were characterized by X-ray diffraction, N_2 adsorption−desorption isotherms, scanning electron microscopy, transmission electron microscopy, Fourier transform infrared, and X-ray photoelectron spectroscopy. The physicochemical characterization results show that all of the samples have well-ordered cubic mesostructures and that the structural integrity is preserved for n_{Si}/n_{Co} ratios as high as 10. It was found that most of the cobalt ions exist as isolated framework species, but for Co-KIT-6 with an n_{Si}/n_{Co} ratio of 10, the presence of extra-framework species/small cobalt oxide clusters cannot be excluded. The ability of these catalysts was tested by examining the conversion of the reaction of methylcyclopentane with hydrogen at atmospheric pressure and temperatures between 200 and 450 °C. The catalytic results show that their catalytic activity increases significantly with increasing cobalt content. The active sites, tetrahedrally coordinated Co and isolated atomic Co sites, were responsible for the endocyclic C−C bond rupture between substituted secondary−tertiary carbon atoms, whereas the small clusters serve as active sites for the successive C−C bond rupture. The ring-opening selectivity can be improved by increasing the density of isolated cobalt atom sites at low reaction temperatures.

R É S U M É

Les matériaux mésoporeux Co-KIT-6, avec une symétrie $Ia3d$ et des rapports Si/Co de 50, 25 et 10, ont été préparés par voie directe en utilisant la synthèse hydrothermale. Les matériaux mésoporeux Co-KIT-6 ont été caractérisés par sorption d'azote, DRX,

☆ This article is part of the thematic issue dedicated to the scientific work of François G. Gault.

* Corresponding author.
E-mail addresses: ifechete@unistra.fr, i_fechete@yahoo.com (I. Fechete).

Ouverture du cycle
n-H
Rupture endocyclique de liaison C–C

microscopies MET et MEB, FT-IR et XPS. Les résultats de la caractérisation physicochimique montrent que tous les échantillons ont une mésostructure cubique bien ordonnée et que l'intégrité structurale est conservée pour des rapports $n_{Si}/n_{Co} > 10$. On a constaté que la plupart des ions cobalt existent comme atomes isolés. En revanche, pour Co-KIT-6 avec un rapport n_{Si}/n_{Co} de 10, la présence d'espèces extra-charpentes/petits amas d'oxyde de cobalt ne peut être exclue. Les performances catalytiques de ces catalyseurs ont été testées en examinant la réaction de conversion du méthylcyclopentane (MCP) avec de l'hydrogène, à la pression atmosphérique et des températures entre 200 et 450 °C. Les résultats catalytiques montrent que leur activité catalytique augmente significativement avec l'augmentation de la teneur en cobalt. Les sites actifs, le Co tétraédriquement coordonné et les sites de Co atomiques isolés, sont responsables de la rupture de la liaison C–C endocyclique entre les atomes de carbone secondaire–tertiaire substitués, tandis que les petits amas de Co servent de sites actifs pour les ruptures successives des liaisons C–C. La sélectivité pour l'ouverture de cycle peut être améliorée en augmentant la densité des sites d'atomes isolés de cobalt, à basse température de réaction.

1. Introduction

For the petrochemical industry, the ring opening of methylcyclopentane (MCP) can be performed with atom efficiency (100% selectivity) on noble metal catalysts. This reaction is a key factor for increasing the cetane number of diesel fuel [1–6] and producing fuel of high quality with minimal harmful emissions. The ring opening of MCP is one of the most-used model reactions for exploring the structural sensitivity of hydrocarbon conversion catalyzed by noble metals [1–7]. More exactly, taking into account that each dearomatization reaction followed by a hydrogenation step leads to a cyclopentane, the MCP chemistry is very important [8]. Although MCP is not a component of diesel fuel, the ring opening of MCP must first be understood because it serves as a *model molecule* and provides the basis for understanding the behavior of all other molecules [1–8]. The noble metals capable of opening MCP with atom efficiency are Pt, Rh, Ru, and Ir [4–7,9–11], although it is very important to stress that not all of these metals exhibit ring-opening products with high cetane numbers. The ring-opening products of MCP are branched (2-methylpentane, 2-MP; 3-methylpentane, 3-MP) and linear paraffins (n-hexane, n-H), with the latter having the higher cetane number and therefore being the desired product. Pt catalysts can open MCP by breaking either the substituted or the unsubstituted C–C bond of MCP [9]. The difference between the two directions of opening is governed by the dispersion of Pt metal on the Al_2O_3 support. On highly dispersed Pt/Al_2O_3 ($d < 2$ nm), the rupture of substituted C–C bonds is favored due to a π-allyl mechanism, which requires a flat adsorption of three neighboring carbon atoms interacting with a single metal site on the catalyst surface. Thus, the products obtained from opening of MCP on highly dispersed catalyst were 2-MP, 3-MP, and n-H. On poorly dispersed Pt/Al_2O_3 ($d > 2$ nm) the preferential rupture of the unsubstituted C–C bond takes place. This can be attributed to a dicarbene mechanism where two endocyclic carbon atoms are involved with adjacent metal

atoms. In this case, the reaction products are only 2-MP and 3-MP, not n-H. Opposite behavior was observed on Ir catalysts, which were found to be insensitive to the dispersion of particles (2-MP and 3-MP products only) [9,11–15]. In addition, Ir catalysts exhibited the tendency to break the endocyclic C–C bonds of MCP on unsubstituted secondary–secondary carbon atoms [9]. In this case, the ring opening of MCP is mainly via a dicarbene mechanism in which the intermediate products adsorb perpendicularly to the metal surface. Nevertheless, these results are not absolute because other catalytic results on Ir catalysts of different dispersions [13] broke the endocyclic C–C bond of MCP on the substituted C–C bonds when the catalysts became covered with carbon species [16–18]. In this case, a plausible explanation was the presence of carbon species that could suppress the dicarbene mechanism. Contrary to alumina support making the breakage of endocyclic C–C bonds on substituted positions possible, the prevailing dicarbene mechanism was observed on Ir catalysts when silica was used as the support [19]. The aim of this study was to find a $Pt–Ir/Al_2O_3$ bimetallic catalyst with the ability to convert molecules with low cetane numbers, such as MCP, to higher value cetane number molecules (e.g., 2-MP, 3-MP, and n-H) at low temperature and with good atom efficiency for diesel fuel applications.

However, new generation ring-opening catalysts are a necessity due to increasing stringent regulations. Many approaches have been pursued to achieve this challenging task, among which the testing mesoporous catalysts with much interest is an important one [8,20–24]. The discovery of mesoporous materials has attracted intense interest because of their high-specific surface area, uniform pore size distributions, and their highly valuable potential applications in catalysis, separation, and adsorption [25–32]. Cobalt-mesoporous catalyst sieves have received intense interest because of their high potential to catalyze various reactions. Is a necessity to prepare uniformly distributed and preferably isolated sites on silica surfaces, which is crucial for high activity and

selectivity but the controlled synthesis of well-defined cobalt species in amorphous silica supports remains a challenge.

The aim of this study was to find a Co-KIT-6 catalyst with the ability to convert molecules with low cetane numbers, such as MCP, to higher value cetane number molecules (e.g., 2-MP, 3-MP, and n-H) at low temperature and with good atom efficiency for diesel fuel applications.

2. Experiment section

2.1. Materials

All chemicals were used as received without further purification. Millipore water was used in all the experiments.

Pluronic P123 [poly(ethylene glycol)–poly(propylene glycol)–poly(ethylene glycol) triblock copolymer, $EO_{20}PO_{70}EO_{20}$, MW 5800, Sigma–Aldrich] and 1-butanol (BuOH, 99.5%, Fluka) were used as the structure-directing agents. Tetraethyl orthosilicate (Si(OC$_2$H$_5$)$_4$, 98%, Sigma–Aldrich) and cobalt acetylacetonate (99%, Aldrich) were used as the silicon and cobalt precursors, respectively. Hydrochloric acid (HCl, 35%, Sigma–Aldrich) was used as the acid source.

Hydrogen, helium, nitrogen, carbon dioxide, and air were purchased from Air Liquide. MCP was supplied by Aldrich (purity >99.99%).

2.2. Synthesis of Co-KIT-6 mesoporous materials

Co-KIT-6 mesoporous materials with different n_{Si}/n_{Co} ratios were prepared by an adapted version of a direct hydrothermal synthesis procedure for Si-KIT-6 [23,33]. The synthesis procedure involved adding 3 g of the amphiphilic triblock copolymer Pluronic P123 and 108.5 g of distilled water to 5.9 g of concentrated HCl (35%). When P123 was completely dissolved, 3 g of butanol was added under stirring at 35 °C. After 1 h of stirring, 6.45 g of tetraethyl orthosilicate and the required amount of cobalt acetylacetonate in 1.5 ml ethanol were added dropwise to the clear homogeneous solution. The resulting gel was stirred at 35 °C for 24 h and subsequently warmed at 100 °C for 24 h under static conditions in a closed polypropylene bottle. The products obtained from the hydrothermal treatment were filtered and dried for 30 h at room temperature. To remove the template, the dried materials were extracted in an ethanol–HCl mixture and then calcined in a programmable oven for 5 h in air (25–550 °C; heating rate 1 °C/min).

2.3. Catalyst characterization

The n_{Si}/n_{Co} molar ratios of the solids were determined by inductively coupled plasma (ICP) atomic emission spectroscopy at the Service Central d'Analyse of CNRS-Solaize. Powder X-ray diffraction (XRD) measurements were performed in an ambient atmosphere using a Bruker D8 Advance powder diffractometer operating in the reflection mode with Cu Kα (λ = 1.5418 Å) radiation, a 40 kV beam voltage, and a 40 mA beam current. The samples were scanned from 0.5° to 4° for the small-angle measurements and from 10° to 90° for the wide-angle measurements using a step size of 0.02° and step time of 10 s. The textural properties, including the BET (Brunauer–Emmett–Teller) specific surface area (S_{BET}), specific pore volume (V_p), and pore diameter (D_p), were determined from low-temperature N$_2$ adsorption–desorption measurements collected using an ASAP 2010 Micrometrics apparatus. Before the analysis, the samples were degassed under vacuum at 130 °C. Scanning electron microscopy (SEM) images were obtained using a Philips XL 30 FEG electron microscope operating at 200 kV. The sample was dispersed as a thin film on a holly carbon grid and sputtered with a thin gold film (5 nm thick) to minimize charging effects. Transmission electron microscopy (TEM) images were obtained using a TopCon 2100 FCs microscope operated at 200 kV.

The Fourier transform infrared (FT-IR) spectra of the samples were recorded in the mid-infrared (IR) region (4000–400 cm^{-1}) using a Nicolet Impact 400 spectrometer. The resolution was 4 cm^{-1}, and 128 scans were collected using the KBr pellet technique. X-ray photoelectron spectroscopy (XPS) spectra were recorded using a Multilab 2000 spectrometer equipped with Al Kα X-ray radiation (1486.6 eV) at an anode current of 20 mA and 10 keV. The XPS analyses were performed in a static system, and the base pressure during the analysis was 10^{-9} Pa. The binding energies obtained from the Co, O, and Si photoelectron peaks were corrected for charging effects by referencing them to the C 1s peak at 284.6 eV.

2.4. Catalytic testing

MCP was reacted under atmospheric pressure in the temperature range of 200–450 °C using a pulse method. Before the catalytic tests, the catalysts were reduced in situ under an H$_2$ flow (40 ml/min) for 4 h at 500 °C (heating rate 5 °C/min). The gas flow used for the catalytic tests was fixed at 40 cm^3 min^{-1}. The catalyst mass was 200 mg, and the volume of MCP injected into the reactor was 5 μl. The C$_1$–C$_6$ products were analyzed by online gas chromatography (GC-2010 Plus, Shimadzu) using a capillary column and flame ionization detector.

3. Results and discussion

3.1. Synthesis of Co-KIT-6. Effect of the n_{Si}/n_{Co} ratio

The morphologies of the Co-KIT-6 catalysts with different n_{Si}/n_{Co} ratios were analyzed using SEM (Fig. 1). The SEM images of the Co-KIT-6 samples with low ($n_{Si}/n_{Co} = 50$) and high cobalt ($n_{Si}/n_{Co} = 10$) loadings are similar, suggesting that incorporating a large amount of cobalt into the structure does not affect strongly the catalyst morphology. All the catalysts are composed of dense, rock-like aggregates.

Fig. 2 shows TEM images of Co-KIT-6 (Si/Co = 25). Uniform pores in KIT-6 are clearly visible and no damage has been incurred in the pore arrangement by isomorphous substitution.
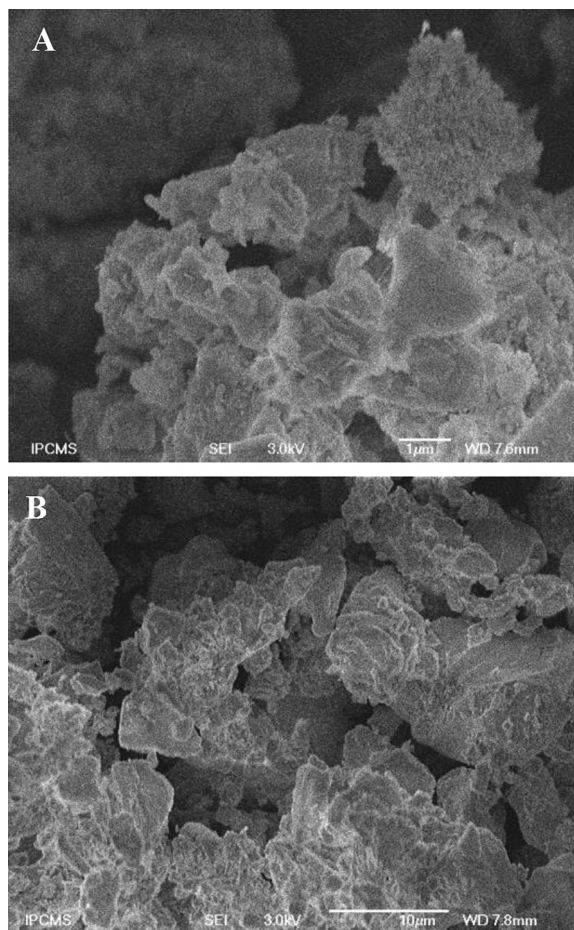
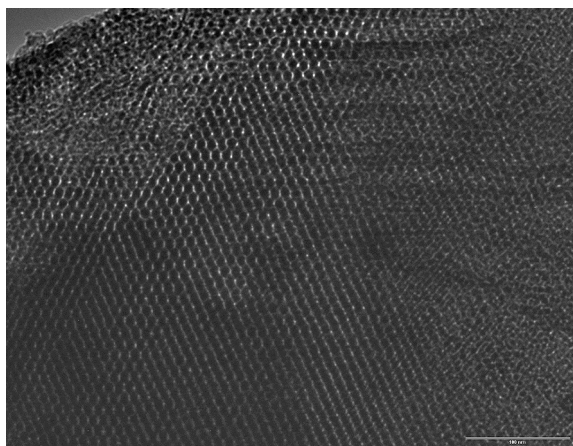**Fig. 1.** SEM images of Co-KIT-6 catalysts with $n_{Si}/n_{Co} = 50$ (a) and $n_{Si}/n_{Co} = 10$ (b).

Fig. 2. TEM images of Co-KIT-6 catalyst with $n_{Si}/n_{Co} = 25$.

The n_{Si}/n_{Co} molar ratios of the calcined materials are listed in Table 1 and compared to the n_{Si}/n_{Co} values of the synthesis gel. The n_{Si}/n_{Co} molar ratios in the calcined materials, obtained from the ICP and XPS analysis, are higher than those in the synthesis gel. However, a slight increase in the Si/Co ratio, from XPS, was observed compared with the chemical analysis.

Fig. 3 shows the small-angle powder X-ray diffractogram of Co-KIT-6 samples with different n_{Si}/n_{Co} ratios after calcination. All the samples have two well-resolved reflections, (211) and (220), which are associated with the $Ia3d$ symmetry of the cubic-ordered pore structure. The small-angle XRD patterns of the Co-KIT-6 ($n_{Si}/n_{Co} = 50$) samples have strong first-order reflections, which are characteristics of KIT-6 materials [23,33], confirming that the cubic structure is preserved after the addition of cobalt. However, the first-order d_{211} peak intensities of the Co-KIT-6 ($n_{Si}/n_{Co} = 25$) and Co-KIT-6 ($n_{Si}/n_{Co} = 10$) samples, which have higher cobalt contents, decrease relative to that of Co-KIT-6 ($n_{Si}/n_{Co} = 50$). These results indicate that the reflections are not highly ordered and these samples are structurally distorted due to interactions between the cobalt and silica species when cobalt is incorporated into the framework. X-ray absorption of the cobalt species might also contribute to this effect. Increasing the amount of cobalt in the materials leads to a shift in the reflection peak position of the Co-KIT-6 ($n_{Si}/n_{Co} = 10$) catalyst to a lower angle than that of Co-KIT-6 ($n_{Si}/n_{Co} = 50$). The shift in the d_{211} peak to a lower angle and its broadening with increasing cobalt content reveal that the lattice expands and the d-spacing increases when cobalt is incorporated into the KIT-6 framework. The unit cell parameter increases from 3.96 for Co-KIT-6 ($n_{Si}/n_{Co} = 50$) to 4.29 for Co-KIT-6 ($n_{Si}/n_{Co} = 10$) as more cobalt is introduced into the KIT-6 framework. The increase in the unit cell parameter with decreasing n_{Si}/n_{Co} ratio is consistent with tetrahedrally coordinated cobalt atoms in the KIT-6 silica framework. It is expected that the unit cell parameter will increase when metal cations are incorporated into the structure because the ionic radius of cobalt is larger than that of Si, resulting in a longer Co–O bond than Si–O bond. Thus, the larger ionic radius and longer Co–O bond lead to an increase in the unit cell parameter (a_0) (Table 1). Similar results have also been reported for metal-substituted mesoporous materials [34,35].

The crystalline cobalt phases are not detected in the wide-angle XRD patterns (Fig. 4) of Co-KIT-6 ($n_{Si}/n_{Co} = 50$), Co-KIT-6 ($n_{Si}/n_{Co} = 25$), and Co-KIT-6 ($n_{Si}/n_{Co} = 10$) catalysts, suggesting that either the metal species are homogeneously dispersed on the support or their compositions are below the X-ray scattering coherence length.

The N_2 adsorption–desorption isotherms of calcined catalysts with different n_{Si}/n_{Co} ratios are shown in Fig. 5. The samples exhibit an H_1-type hysteresis loop and a sharp nitrogen capillary condensation step in the P/P_0 range of 0.7–0.8, which is typical for large, uniform mesopores with a narrow pore size distribution. A parallel hysteresis loop, which is characteristic of large, highly ordered mesopores with a uniform pore size distribution, is observed for the Co-KIT-6 ($n_{Si}/n_{Co} = 50$) and Co-KIT-6 ($n_{Si}/n_{Co} = 25$) samples. These results clearly indicate that the catalysts have a uniform textural porosity. The catalysts have type IV isotherms, which is characteristic of ordered mesoporous materials according to the IUPAC classification. However, the height of the Co-KIT-6 ($n_{Si}/n_{Co} = 10$) hysteresis loop is smaller due to

Table 1
Effect of the n_{Si}/n_{Co} ratios on the structural and textural properties of the calcined Co-KIT-6 catalysts.

Sample	n_{Si}/n_{Co}			T (°C)	t (h)	a_0^c (nm)	S_{BET}^d (m²/g)	$V_p,^e$ BJH (cm³/g)	$D_p,^f$ BJH (nm)	w^g (nm)
	Gel	Calcined[a]	XPS[b]							
Co-KIT-6 ($n_{Si}/n_{Co}=50$)	50	62	69	100	24	20.52	800	1.08	6.3	3.96
Co-KIT-6 ($n_{Si}/n_{Co}=25$)	25	29	36	100	24	21.00	690	1.03	6.5	4.00
Co-KIT-6 ($n_{Si}/n_{Co}=10$)	10	14	22	100	24	21.78	408	0.75	6.6	4.29

[a] Obtained from ICP analysis.
[b] Obtained from XPS analysis.
[c] Unit cell parameter was calculated based on the XRD results corresponding to the 3D cubic pore structure with a $Ia3d$ space group, $a_0 = d_{hkl}\sqrt{(h^2 + k^2 + l^2)}$, where d_{hkl} diffraction values were evaluated using the interplanar spacing of the (211) XRD peak.
[d] Specific surface area obtained from N_2 sorption isotherm studies.
[e] Pore volume obtained from N_2 sorption isotherm studies.
[f] Mesopore diameter obtained from N_2 sorption isotherm studies.
[g] Pore wall thickness calculated from formula: $(a_0/2) - D_p$.
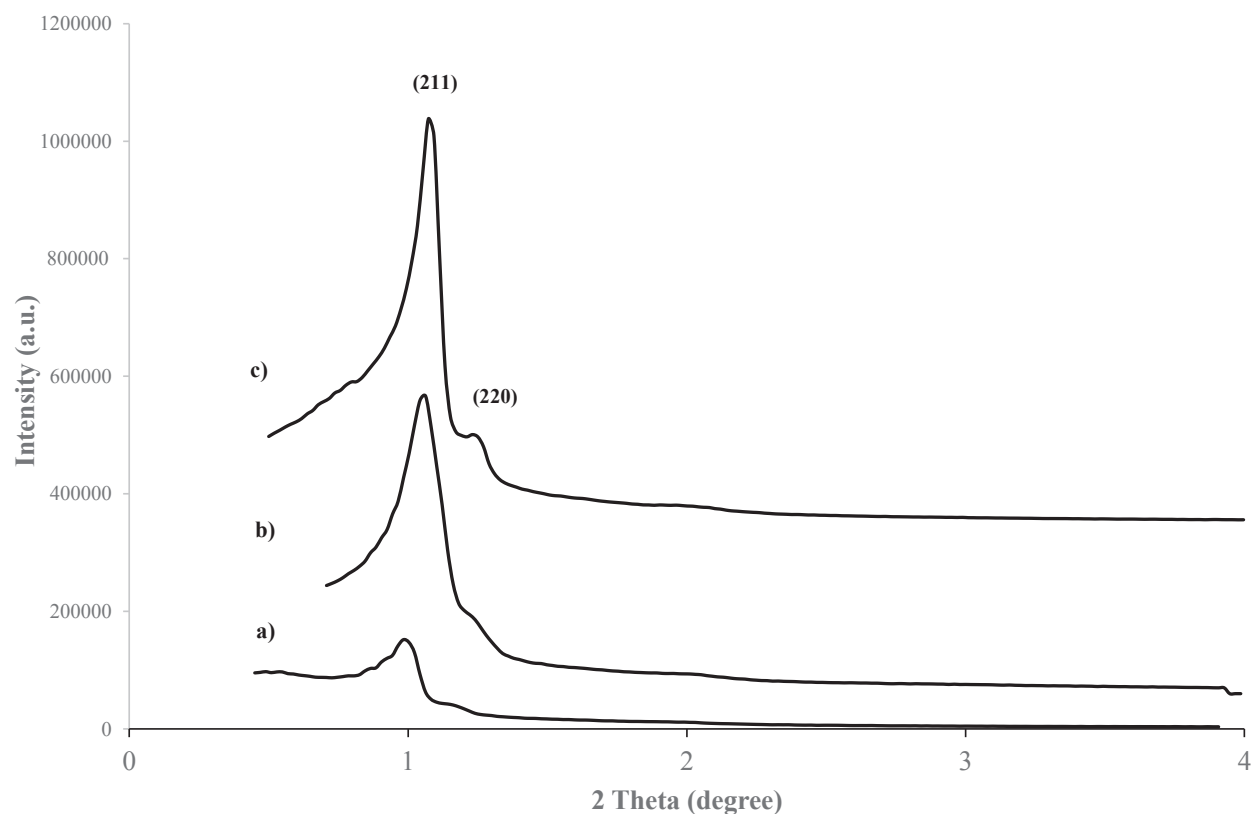
Fig. 3. Small-angle XRD patterns of Co-KIT-6 catalysts synthesized at 100 °C for 24 h with $n_{Si}/n_{Co} = 10$ (a), $n_{Si}/n_{Co} = 25$ (b), and $n_{Si}/n_{Co} = 50$ (c).

high metal loading in the mesopores. The inflection point shifts slightly to higher relative pressures as more metal is incorporated in the structure, indicating that the pore size increases. The specific surface area (S_{BET}), cumulative pore volume (V_p), and pore diameter (D_p) of the Co-KIT-6 catalysts are listed in Table 1. The smaller values for the Co-KIT-6 ($n_{Si}/n_{Co} = 10$) sample might be due to the decrease in its structural ordering. However, the reduction in the pore volume with increasing Co content might be due to the obstruction of some of the Co-KIT-6 mesoporous channels with cobalt oxide species during calcination. It should be noted that these parameters do not vary much with cobalt

content for the Co-KIT-6 ($n_{Si}/n_{Co} = 50$) and Co-KIT-6 ($n_{Si}/n_{Co} = 25$) samples. These parameters only decrease significantly for the Co-KIT-6 ($n_{Si}/n_{Co} = 10$) sample, presumably because of the presence of a significant amount of cobalt. These data were combined with the XRD results to estimate the wall thickness of the Co-KIT-6 catalysts. The wall thickness of the Co-KIT-6 catalysts increases with increasing cobalt content (Table 1).

The FT-IR absorption spectra of the calcined mesoporous Co-KIT-6 samples are shown in Fig. 6 as a function of the cobalt loading. In the hydroxyl region, all the samples exhibit a broad absorption band centered at approximately
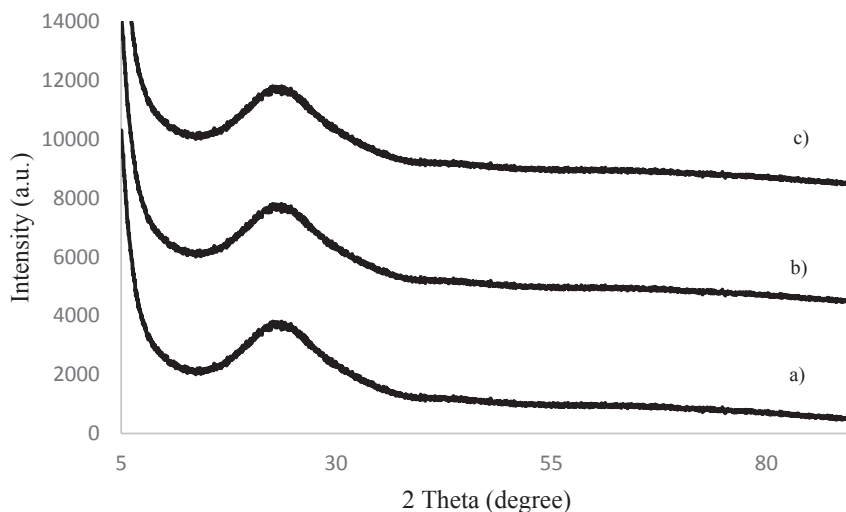
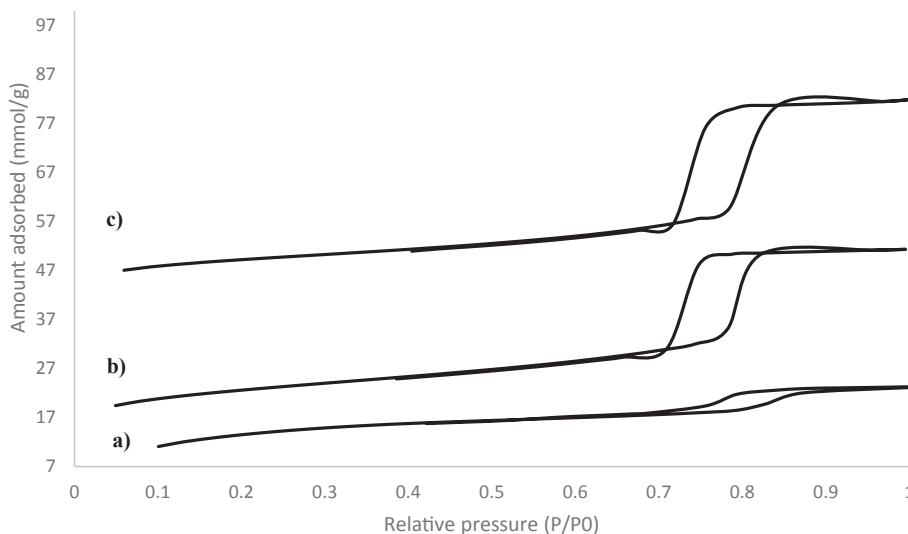**Fig. 4.** Wide-angle XRD patterns of the Co-KIT-6 samples with n_{Si}/n_{Co} ratios of 10, 25, and 50.

Fig. 5. N_2 adsorption–desorption isotherms of Co-KIT-6 catalysts synthesized at 100 °C for 24 h with $n_{Si}/n_{Co} = 10$ (a), $n_{Si}/n_{Co} = 25$ (b), and $n_{Si}/n_{Co} = 50$ (c).
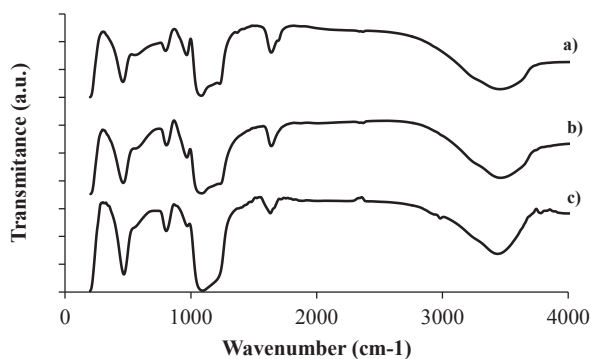

Fig. 6. FT-IR spectra of Co-KIT-6 catalysts synthesized at different n_{Si}/n_{Co} ratios: (a) Co-KIT-6 ($n_{Si}/n_{Co} = 10$), (b) Co-KIT-6 ($n_{Si}/n_{Co} = 25$), and (c) Co-KIT-6($n_{Si}/n_{Co} = 50$).

3455 cm^{-1} attributable to the O–H stretching vibrations of water molecules adsorbed on the mesoporous Co-KIT-6 surfaces. The weak band at approximately 1635 cm^{-1} is assigned to the bending vibrations of adsorbed water molecules. In the framework region, absorption bands are detected at 1100 (the shoulder at 1215 cm^{-1}), 960, 812, and 455 cm^{-1} for all the samples. The presence of these bands confirms that the mesoporous Co-KIT-6 framework is formed and the structural properties are unchanged despite the isomorphous substitution of Co for Si up to an n_{Si}/n_{Co} ratio of 10. The absorption band at 1100 cm^{-1}, the shoulder at 1215 cm^{-1}, and the band at 812 cm^{-1} are assigned to the asymmetric and symmetric stretching vibrations of the structural siloxane (Si–O–Si) group, whereas the band at 455 cm^{-1} is attributed to the Si–O–Si and Si–O–Co bending vibrations in the mesoporous

framework (i.e., the SiO$_4$ tetrahedron vibrations) [36]. The band at 960 cm^{-1} is usually attributed to silanol (Si–OH) groups in the mesoporous solid framework or to a stretching mode of a [SiO$_4$] unit bonded to cobalt atoms [37]. However, for the Co-KIT-6 ($n_{Si}/n_{Co} = 25$) and Co-KIT-6 ($n_{Si}/n_{Co} = 10$) samples, this band can be attributed to the presence of Si–O–Co groups and indicates that the cobalt atoms are incorporated into the mesoporous Co-KIT-6 framework. These results show that high cobalt loadings do not affect the Co-KIT-6 framework structure.

The oxidation state of cobalt was investigated by XPS (Fig. 7). The n_{Si}/n_{Co} molar ratios calculated from the integral intensities of the Si 2p and Co 2p photoelectron spectra are included in Table 1. The surface n_{Si}/n_{Co} molar ratios are slightly higher than the bulk ratios calculated from the chemical analysis. The binding energy of Co 2p$_{3/2}$ of Co-KIT-6 was 780.5 eV, and the cobalt species can be assigned to Co(II) in an isolated state [38,39].

3.2. Catalytic reactivity

The MCP conversion of Co-KIT-6 catalysts with different n_{Si}/n_{Co} ratios is presented as a function of the reaction temperature in Table 2. The conversions of all the studied catalysts are temperature dependent. The catalysts are active in the temperature range of 200–450 °C and have similar product distributions. The dominant products are methane (C1) and n-H, and Bz is observed only at high temperatures for Co-KIT-6 with high cobalt content (Si/Co of 10).

The total conversion increases with increasing reaction temperature. It should be noted that at a given temperature, the catalytic activity increases with increasing cobalt content. The Co-KIT-6 ($n_{Si}/n_{Co} = 10$) and Co-KIT-6 ($n_{Si}/n_{Co} = 25$) catalysts exhibit MCP conversions of 3.7% and 0.93%, respectively, at 200 °C. These results suggest that the catalytic activity is an inherent property of the Co-doped mesoporous structure and is strongly dependent on the active site density in the mesoporous matrix, as previously observed in other catalytic systems [20–24].

At low temperatures between 200 and 300 °C, the ring-opening selectivity is 100%, and n-H is the only product for all the catalysts, except for Co-KIT-6($n_{Si}/n_{Co} = 10$), which has a ring-opening selectivity of 80%. Furthermore, the ring-opening selectivity decreases at 350 °C, but ring

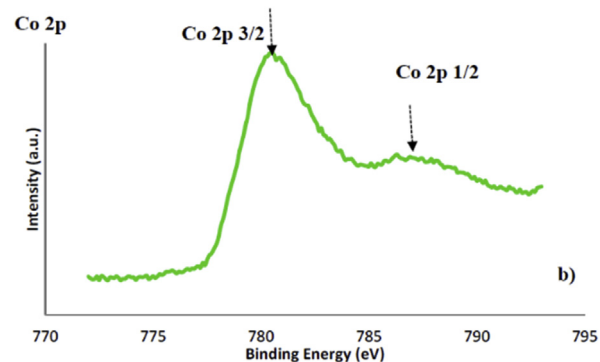**Fig. 7.** XPS spectra of Co-KIT-6 ($n_{Si}/n_{Co} = 10$) catalysts.

Table 2
Effect of the n_{Si}/n_{Co} ratios and temperature on the conversion of MCP.

Sample	T (°C)	X_T (%)	S_{RO}, n-H (%)	S_C, C$_1$ (%)	S_{RE}, Bz (%)
Co-KIT-6 ($n_{Si}/n_{Co} = 50$)					
	200	0.45	100	0	0
	250	0.97	100	0	0
	300	2.47	100	0	0
	350	8.20	100	0	0
	400	16.2	69	31	0
	450	23.2	29	71	0
Co-KIT-6 ($n_{Si}/n_{Co} = 25$)					
	200	0.93	100	0	0
	250	3.7	100	0	0
	300	6.6	100	0	0
	350	14.7	74	26	0
	400	26.9	30	70	0
	450	40.6	11	89	0
Co-KIT-6 ($n_{Si}/n_{Co} = 10$)					
	200	3.7	100	0	0
	250	6.4	100	0	0
	300	14.2	80	20	0
	350	27	59	41	0
	400	38	24	76	0
	450	56	9	84	7

X_T, total conversion of MCP; S_{RO}, ring-opening selectivity; S_C, cracking selectivity; S_{RE}, ring enlargement selectivity. The catalyst samples were reduced under an H$_2$ flow (40 ml/min) for 4 h at 500 °C (heating rate 5 °C/min); $m_{catalyst} = 200$ mg; V_{MCP} injected = 5 μl. The gas flow used for the catalytic tests was fixed at 40 cm^3 min^{-1}.

opening is still the dominant conversion pathway. The selectivity to n-H at this low temperature and the low conversion observed in the absence of secondary reactions demonstrate the intrinsic ability of the catalysts to break endocyclic substituted C–C bonds. It appears that the C–C bond rupture primarily produces n-H. However, n-H formation is observed between 200 and 450 °C, which suggests that the isolated, tetrahedrally coordinated cobalt active sites preferentially induce the rupture of endocyclic substituted C–C bonds in the temperature range studied. At high temperatures and high cobalt loadings, the ring-opening selectivity decreases as the cracking selectivity (C$_1$) increases. C$_1$ is formed by the successive rupture of C–C bonds through the subsequent reactions of intermediate products. At high temperatures, all the catalysts actively convert MCP, but they are not selective for the ring-opening reaction. Most likely, the heat of adsorption on the Co-KIT-6 active sites is large, favoring multiple C–C bond-breaking reactions.

These results show that at low reaction temperatures, all the catalysts are active and selective for MCP ring opening to form n-H exclusively. As the cobalt loading increases, the activity and selectivity of the studied catalysts also decrease in the following order: Co-KIT-6($n_{Si}/n_{Co} = 10$) > Co-KIT-6($n_{Si}/n_{Co} = 25$) > Co-KIT-6($n_{Si}/n_{Co} = 50$). The formation of large amounts of n-H might require a high density of isolated tetrahedral cobalt active sites for endocyclic C–C bond rupture.

4. Conclusions

Highly ordered mesoporous Co-KIT-6 with a bicontinuous cubic *Ia*3*d* structure was successfully synthesized using a hydrothermal approach. The physicochemical

characterization shows that the structural integrity is preserved for cobalt loadings of up to an n_{Si}/n_{Co} ratio of 10.

The catalytic studies indicate that Co-KIT-6 with various Si/Co ratios exhibited outstanding ring-opening selectivity. Among the ring-opening products, n-H was formed exclusively. The ring-opening selectivity can be improved by increasing the density of atomically isolated cobalt sites. The cobalt loading governs the cobalt coordination environment, that is, the nature and structure of the cobalt species. Low temperatures favor high selectivity (100%) to n-H by endocyclic C–C bond rupture.

Acknowledgments

References

[1] P. Zeuthen, U.S. Patent 6,235,962, 2001.
[2] G. B. Vicker, W. C. Baird Jr, J. G. Chen, U.S. Patent 6,623,625, 2003.
[3] H. Du, C. Fairbridge, H. Yang, Z. Ring, Appl. Catal. A 294 (2005) 1.
[4] A. Djeddi, I. Fechete, O. Ersen, F. Garin, C. R. Chimie 16 (2013) 433.
[5] A. Djeddi, I. Fechete, F. Garin, Appl. Catal. A 413–414 (2012) 340.
[6] A. Djeddi, I. Fechete, F. Garin, Catal. Commun. 17 (2012) 173.
[7] A. Djeddi, I. Fechete, F. Garin, Top. Catal. 55 (2012) 700.
[8] S. Haddoum, I. Fechete, B. Donnio, F. Garin, D. Lutic, C.E. Chitour, Catal. Commun. 27 (2012) 141.
[9] F.G. Gault, Adv. Catal. 30 (1981) 1.
[10] D. Teschner, Z. Paal, React. Kinet. Catal. Lett. 68 (1999) 25.
[11] G.B. McVicker, M. Daage, M.S. Touvelle, C.W. Hudson, D.P. Klein, W.C. Baird Jr., B.R. Cook, J.G. Chen, S. Hantzer, D.E.W. Vaughan, E.S. Ellis, O.C. Feeley, J. Catal. 210 (2002) 137.
[12] G. Maire, G. Plouidy, J.C. Prudhomme, F.G. Gault, J. Catal. 4 (1965) 556.
[13] J.G. van Senden, E.H. van Broekhoven, C.T.J. Wreesman, V. Ponec, J. Catal. 87 (1984) 468.
[14] F. Weisang, F.G. Gault, Chem. Commun. 11 (1979) 519.
[15] Y. Barron, G. Maire, J.M. Muller, F.G. Gault, J. Catal. 5 (1966) 428.
[16] E. Fulop, V. Gnutzmann, Z. Paal, V. Vogel, Appl. Catal. 66 (1990) 319.
[17] M. Chow, G.B. McVicker, J. Catal. 112 (1988) 303.
[18] F.J. Schepers, E.H. van Broekhoven, V. Ponec, J. Catal. 96 (1985) 82.
[19] T. Do, W.E. Alvarez, D.E. Resasco, J. Catal. 238 (2006) 477.
[20] I. Fechete, B. Donnio, O. Ersen, T. Dintzer, A. Djeddi, F. Garin, Appl. Surf. Sci. 257 (2011) 2791.
[21] I. Fechete, S. Debbih-Boustila, R. Merkache, O. Hulea, L. Lazar, D. Lutic, I. Balasanian, F. Garin, Environ. Eng. Manag. J. 11 (2012) 1931.
[22] R. Merkache, I. Fechete, M. Bernard, P. Turek, K. Al-Dalama, F. Garin, Appl. Catal. A 504 (2015) 672.
[23] A. Boulaoued, I. Fechete, B. Donnio, M. Bernard, P. Turek, F. Garin, Microp. Mesop. Mater. 155 (2012) 131.
[24] I. Fechete, O. Ersen, F. Garin, L. Lazar, A. Rach, Catal. Sci. Technol 3 (2012) 444.
[25] I. Fechete, J.C. Védrine, Molecules 20 (2015) 5638.
[26] N. Bensacia, I. Fechete, S. Moulay, O. Hulea, A. Boos, F. Garin, C. R. Chimie 17 (2014) 869.
[27] SSSC.
[28] I. Fechete, J.C. Védrine, C. R. Chimie 19 (2016) 1203.
[29] O.M. Ishchenko, S. Krishnamoorthy, N. Valle, J. Guillot, O. Turek, I. Fechete, D. Lenoble, J. Phys. Chem. C 120 (2016) 7067.
[30] B.J. Scott, G. Wirnsberger, G.D. Stucky, Chem. Mater. 13 (2001) 3140.
[31] K. Ariga, A. Vinu, Y. Yamauchi, Q. Ji, J.P. Hill, Bull. Chem. Soc. Jpn. 8 (2012) 132.
[32] E. Pellicer, J. Sort, Nanomater 6 (2016) 15.
[33] F. Kleitz, S.H. Choi, R. Ryoo, Chem. Commun. (2003) 2136.
[34] A. Ramanathan, R. Maheswari, D.H. Barich, B. Subramaniam, Microporous Mesoporous Mater. 190 (2014) 240.
[35] A. Prabhu, A. Al Shoaibi, C. Srinivasakannan, Appl. Catal. A 466 (2013) 137.
[36] B.-G. Park, W. Guo, X. Cui, J. Park, C.-S. Ha, Microporous Mesoporous Mater. 66 (2003) 229.
[37] T. Blasco, A. Corma, M.T. Navarro, J.P. Pariente, J. Catal. 156 (1995) 65.
[38] L. Guczi, D. Bazin, Appl. Catal. A 188 (1999) 163.
[39] S.W. Ho, M. Horialla, D.M. Hercules, J. Phys. Chem. 94 (1990) 6396.